Coordinatively labile 18-electron arene ruthenium iminophosphonamide complexes

Iana Sinopalnikova, Tatyana A. Peganova, Valentin V. Novikov, Ivan V. Fedyanin, O. A. Filippov, N. V. Belkova, E. S. Shubina, Rinaldo Poli, Alexander M. Kalsin

Coordinatively labile 18-electron arene ruthenium iminophosphonamide complexes

Iana S. Sinopalnikova,[a,b] Tat'yana A. Peganova,[a] Valentin V. Novikov,[a] Ivan V. Fedyanin,[a] Oleg A. Filippov,[a] Natalia V. Belkova,[a] Elena S. Shubina,[a] Rinaldo Poli,[b,c] Alexander M. Kalsin*[a]

Abstract: The thermodynamics of chloride dissociation from the 18ē arene ruthenium iminophosphonamides [(η^6-arene)RuCl{(R'N)$_2$PR$_2$}] (**1a-d**) (previously known systems with arene = C_6Me_6, R = Ph, R' = *p*-Tol (**a**); R = Et, R' = *p*-Tol (**b**); R = Ph, R' = Me (**c**); and new ones with arene = *p*-cymene, R = Ph, R' = *p*-Tol (**d**)) has been assessed in both polar and apolar solvents, using variable-temperature UV-visible, NMR and 2D EXSY ^{1}H NMR methods, highlighting the NPN ligand influence on the equilibrium parameters. The dissociation enthalpy ΔH_d decreases upon increasing the electron-donating ability of the N-,P- substituents (**1a**, **1d** > **1b** > **1c**) and the solvent polarity, resulting in the exothermic spontaneous dissociation of **1c** in polar solvents. The coordination of neutral ligands (MeCN, pyridine, CO) to the corresponding 16ē complexes [(η^6-arene)Ru{(R'N)$_2$PR$_2$}]$^+$(PF_6^-) (**2a-d**) is reversible; the stability of the **2·L** adducts depends on the L π-accepting ability. Carbonylation of **2a** and **2d** results rare examples of cationic arene ruthenium carbonyl complexes (**3a**, **3d**), while the monocarbonyl adduct derived from **2c** reacts further with a second CO molecule, rapidly converting to the carbonyl-carbamoyl complex **3c**, where one CO molecule is inserted into the Ru–N bond. The new complexes **1d**, **2d**, **3a**, **3c** and **3d** were isolated and structurally characterized.

Introduction

Coordinatively unsaturated complexes are often considered as intermediates in various metal-catalyzed organic transformations. Generally the stability of these species correlates with their activity in catalysis, i.e. the more unsaturated species are more reactive, however at the expense of selectivity. Ruthenium complexes are known to catalyze numerous organic reactions[1] of substrates bearing various functional groups, to which a catalyst must be tolerant. The reactivity of the unsaturated species thus should be fine-tuned by reducing the electrophilicity of the ruthenium center with the ligand environment. Ligands having extra lone pair at the coordinated heteroatom are capable to partially compensate the electron deficiency of the metal via π-donation.[2] O- and N-ligands usually provide significantly greater stabilization than halides, e.g. following the order $OSiMe_2Ph$ > NHPh > $OSiPh_3$ > OCH_2CF_3 >> Cl > Br > I for half-sandwich [Cp*Ru(X)(PR_3)] complexes.[3] Among the chelating anionic κ^2-N,N-ligands, strongly electron-donating β-diketiminate and zwitterionic bis(imidazoline-2-imine) ligands were found to generate either 18ē complexes with weakened Ru–Cl bonds,[4-6] or very stable 16ē half-sandwich ruthenium complexes that do not coordinate the chloride ion at all.[7,8] The π-donation of the lone electronic pairs at the nitrogen atoms in ruthenium amidinates is limited because of symmetry reasons; it occurs only in the unfavorable conformation with a bent metallacycle and thus the stabilization effect is less pronounced.[9-13] We have recently proposed that structurally similar iminophosphonamide ligands [$R_2P(NR')_2$]$^-$ can efficiently stabilize the coordinatively unsaturated ruthenium complexes, thanks to their zwitterionic structure[14] and therefore to the absence of symmetry restrictions for π-donation.[15] The observation of elongated Ru–Cl bonds (2.44–2.45 Å) in 18ē complexes [(C_6Me_6)RuCl{(RN)$_2$PR'$_2$}] and shortened Ru–N bonds (average 2.01–2.04 Å) in the corresponding 16ē complexes [(C_6Me_6)Ru{(RN)$_2$PR'$_2$}]$^+$(X^-) supports this hypothesis.[15] In 1998 Parsons *et al.* reported the first 16ē ruthenium iminophosphonamide complex [(*p*-Cymene)Ru{(^{i}PrN)$_2$PPh(NH^{i}Pr)}](BPh_4) to be extremely stable and inert to the addition of Cl^-, PPh_3 and $P(OEt)_3$; even the CO adduct could not be isolated due to intrinsic instability.[16] Since then, no 18ē cationic NPN complexes [(arene)Ru(L){(RN)$_2$PR'$_2$}]$^+$ could be isolated, suggesting that the σ,π-donor character of the NPN ligand is too strong to allow stability for such adducts.

Here we report a comprehensive quantitative exploration of reversible coordination of neutral ligands with various π-acceptor capabilities (MeCN, pyridine and CO) to cationic 16ē arene ruthenium iminophosphonamides **2a-d**, and the chloride dissociation from the 18ē complexes **1a-d** (Chart 1), aiming to determine the influence of the arene nature and of the N-, P-substituents in the NPN-ligand on the thermodynamics of ligand coordination/dissociation. These data on the coordination behavior of ruthenium iminophosphonamides are particularly important in view of their potential use in catalysis.

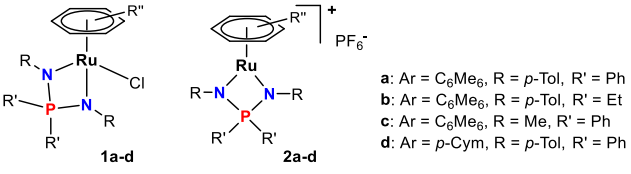

Chart 1.

[a] Ms. Iana S. Sinopalnikova, Dr. Tat'yana A. Peganova, Dr. Valentin V. Novikov, Dr. Ivan V. Fedyanin, Dr. Oleg A. Filippov, Prof. Natalia V. Belkova, Prof. Elena S. Shubina, and Dr. Alexander M. Kalsin*
A.N. Nesmeyanov Institute of Organoelement Compounds
Russian Academy of Sciences
28 Vavilov str., 119991 Moscow, Russia
E-mail: kalsin@ineos.ac.ru

[b] Ms. Iana S. Sinopalnikova and Prof. Rinaldo Poli
Laboratoire de Chimie de Coordination CNRS
Université de Toulouse, UPS, INPT
205 Route de Narbonne, 31077 Toulouse Cedex 4, France

[c] Prof. Rinaldo Poli
Institut Universitaire de France
1, rue Descartes, 75231 Paris Cedex 05, France

Supporting information for this article is given via a link at the end of the document.

Results and Discussion

Synthesis and characterization of the complexes 1d and 2d.

The new *p*-cymene ruthenium NPN-complexes (**1d**, **2d**) were synthesized similarly to their hexamethylbenzene analogues **1a** and **2a**,[15] i.e. by reacting $[(p\text{-cymene})RuCl_2]_2$ with iminophosphonamide **A** after deprotonation with 1 equiv. of NaHMDS to obtain **1d** and further abstraction of the chloride ligand with $AgPF_6$ to yield the corresponding 16ē cationic complex **2d** (Scheme 1). The isolated products were fully characterized by NMR spectroscopy and elemental analysis, and their molecular structures were confirmed by single crystal X-ray diffraction studies (Figures 1 and 2, Table S6 in ESI).

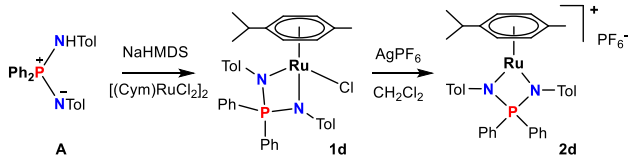

Scheme 1. Synthesis of the complexes **1d**, **2d**.

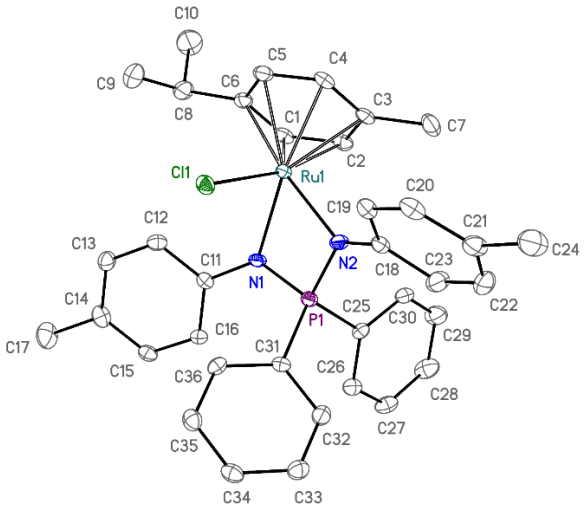

Figure 1. ORTEP diagram of **1d**. Ellipsoids are shown at the 50% probability level; hydrogen atoms are omitted for clarity. Selected bond lengths (Å) and angles (°): Ru···Arene(centroid) 1.667(1), Ru–Cl 2.415(1), Ru–N1 2.145(2), Ru–N2 2.126(3), N1–Ru–N2 68.24(9), Ru–N1–P–N2 178.43(16), Σ(N1) 357.2(6), Σ(N2) 358.2(6).

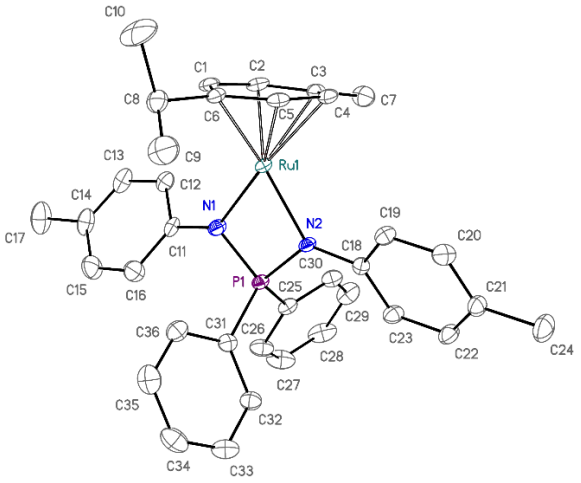

Figure 2. ORTEP diagram of the cation **2d**. Ellipsoids are shown at the 50% probability level; hydrogen atoms and the anion are omitted for clarity. Selected bond lengths (Å) and angles (°): Ru···Arene(centroid) 1.659(1), Ru–N1 2.031(2), Ru–N2 2.017(3), N1–Ru–N2 72.42(10), Ru–N1–P–N2 174.27(15), Σ(N1) 360.0(6), Σ(N2) 358.9(5).

The 18ē complex **1d** exhibits a three-legged piano stool geometry with a pseudo octahedral configuration of the ligands around the ruthenium atom. The structural parameters of **1d** are similar to those of its C_6Me_6 analogues **1a-c**, except for the Ru–N and Ru–Cl distances that are about 0.02 Å shorter (the average Ru–N and Ru–Cl bond lengths in **1a-c** are 2.148–2.156(4) Å and 2.437–2.445(4) Å, respectively).[15] The *p*-cymene ligand is a weaker donor and has lower steric requirements than C_6Me_6, hence the lack of electron density on the ruthenium atom in **1d** is compensated by shortening the bonds with the NPN and Cl ligands. The pyramidalization of the nitrogen atoms, as indicated by Σ(N), is small like for the complexes **1a,b**. This is a result of the ability of the N-tolyl substituents in **1a,b,d** to delocalize the unshared electron density of the nitrogen atoms, in sharp contrast with the severe pyramidalization of one of the nitrogen atoms in **1c** (Σ(N1) = 344.4°), for which such delocalization is impossible.

The 16ē cationic complex **2d** exhibits a two-legged piano-stool geometry with the chelating NPN-ligand positioned nearly perpendicular to the *p*-cymene ligand. Most of the structural parameters of **2d** are similar to those of its C_6Me_6 counterparts **2a,b**, besides less significant distortion of the arene ligand. The *p*-cymene ligand in **2d** is almost planar (Ru–C(arene) bonds in the 2.159–2.204(3) Å range) compared to the C_6Me_6 ring in **2a** and **2b**, which is bent towards a boat conformation with two considerably longer Ru–C(arene) bonds (*trans* to Ru–N; 2.228-2.275(2) Å) *vs*. the other four (2.143-2.201(2) Å).[15] This structural peculiarity may result from weaker back-bonding from the ruthenium atom to the arene ligand in **2d**.

The geometrical differences observed for the C_6Me_6 and *p*-cymene complexes were reproduced by the density functional theory (DFT) calculation performed for **1a**, **1d**, **2a** and **2d** in the gas phase with PBE functional and def2-TZVP basis set. The optimized structures differ from the experimentally determined

ones by <0.03 Å for the distances and <2° for the bond angles (ESI, Tables S7 and S8). It is noteworthy that the DFT calculations also predict the arene orientation relative to the Cl,N,N atoms in **1a** and **1d** (the dihedral angle Cl–Ru–Centroid-C5 differs by <3°). Coordination of the arene ligand in the 16ē complexes **2a** and **2d** has a well-pronounced η^2-η^2 character, with the Ru–C1 and Ru–C4 bonds being ca. 0.04 Å (**2d**) or 0.09 Å (**2a**) longer than the other four Ru–C bonds, which also indicates a stronger distortion of the planar arene ring towards a boat conformation for **2a** than for **2d**. This pattern can be explained by the symmetry of the ruthenium orbitals interacting with the arene ring (see below).

The 16ē complexes **2a-c** exhibit a moderate intensity band in the UV-vis spectra centered at 540-550 nm,[15] which was supposed to belong to a *d*-*d** transition. The UV-Vis spectra of **2d** exhibit a similar band, although surprisingly shifted to longer wavelengths (λ_{max} = 590 nm). According to the calculated orbital pattern of **2a** and **2d**, the highest occupied molecular orbitals (HOMO) (ESI, Fig. S10) of both cations are assigned to the antibonding combination of the ruthenium d_{xy} orbital with the A_2-symmetric group orbital of the NPN ligand (linear combination of the nitrogen atoms p_y orbitals) and are located at very close energies (-7.4 eV in the gas phase and -5.1 eV in CH_2Cl_2 solution, Table 1). In both **2a** and **2d**, the lowest unoccupied molecular orbital (LUMO) (ESI, Fig. S11) is a combination of the ruthenium unoccupied d_{yz} orbital and occupied B_2 π-orbital of the arene ligand. Lowering the energy of the corresponding bonding orbital (HOMO-14, see ESI, Fig. S12) is responsible for the elongation of two C-C bonds (C2–C3 and C5–C6) of the η^6-arene ligand. The greater electron-donating ability of C_6Me_6 leads to a higher energy LUMO by 0.4 eV in **2a** (Table 1). Hence the bands observed at 540 nm (**2a**) and 590 nm (**2d**) in the UV-vis spectra appear consistent with a ligand-to-metal charge-transfer transition, as in the 16ē arene ruthenium dithiolate complexes.[17] The HOMO-LUMO gap for **2a** and **2d** are calculated in CH_2Cl_2 as 2.05 and 1.65 eV (Table 1), respectively, thus reflecting a significant red shift for the absorption of **2d** compared to **2a**.

Table 1. The HOMO, LUMO energies and the HOMO-LUMO gap for **2a** and **2d** calculated in the gas phase and CH_2Cl_2 solution in comparison to the energy of the experimentally observed band (all in eV).

	2a		**2d**	
	Gas phase	CH_2Cl_2	Gas phase	CH_2Cl_2
HOMO	-7.45	-5.06	-7.37	-5.05
LUMO	-5.50	-3.01	-5.92	-3.40
Gap	1.95	2.05	1.45	1.65
Expt		2.32		2.10

It should be noted that the LUMO in complexes **2** is the orbital available to accept the electron pair donated by the external ligand (L or Cl) upon formation of the 18ē adduct. Hence, the lower energy of the LUMO in **2d** is responsible for the stronger bonding of chlorine atom in the *p*-cymene complex *vs* those containing C_6Me_6, as reflected by the computed and measured Ru–Cl bond lengths (Tables S7 and S8).

Coordination lability of complexes 1a-d

Despite the low symmetry (C_1) of **1d** in the solid state, only two doublets at δ 5.05 and 4.87 (C_6D_6) were observed for the coordinated arene in the ^{1}H NMR spectrum, as well as two singlets at δ 79.4, 80.7 in the ^{13}C NMR spectrum, because of facile rotation of the *p*-cymene ring around the Ru–Arene axis yielding an effective C_s symmetry in solution. The NMR spectral feature of **2d** are equally in accord with C_s-symmetry. On the other hand, the ^{1}H and ^{13}C NMR spectra for the P-phenyl substituents of **1d** exhibit the expected two sets of signals in C_6D_6 but only one in $CDCl_3$, suggesting an even higher (effective C_{2v}) point group symmetry in the latter solvent. This can be rationalized, in addition to the rapid *p*-cymene ring rotation around the Ru–Arene axis, by the reversible dissociation of the Ru–Cl bond that yields an equilibrium mixture of the effectively C_{2v}-symmetric intermediate [**2**]$^+$Cl$^-$ and undissociated **1**, as has been previously proposed for **1c**.[15] However, whether this process may occur in apolar solvents and what is the dissociation enthalpy as a function of solvent, NPN substituents and type of arene ligand is still open to question. The additional studies detailed below have brought light on this point.

UV-vis spectroscopic studies of 1b and 1c in polar solvents. As we have previously reported,[15] complex **1c** bearing the most electron-releasing N-Me groups partially dissociates in the relatively polar solutions to give the corresponding cationic species [**2c**]$^+$Cl$^-$ (Scheme 2), as revealed by the strong downfield shift of its ^{31}P NMR resonance in dichloromethane compared to C_6D_6. The detailed study by means of UV-vis spectroscopy revealed the distinct absorption bands in toluene for **1c** (at 430 nm) and **2c** (at 550 nm; ESI, Fig. S1A,B). The spectrum of **1c** in CH_2Cl_2 shows a very broad absorption band located in-between these bands (at 520 nm; Fig. 3), thus suggesting the coexistence of the dissociated and undissociated forms. The spectra are temperature dependent in the range 190-290 K, showing reversible changes with an isosbestic point at λ = 480 nm (Fig. 3). The standard enthalpy and entropy for the dissociation process (Scheme 2) were calculated from the Van't Hoff equation using the T-dependent molar extinction coefficient of **2c** at λ = 600 nm. The dissociation process is exothermic (ΔH_d = -5.0±0.2 kcal/mol), with the cationic form dominating at low temperatures. The unexpectedly large negative entropy change (ΔS_d = -27.0±0.7 cal/(mol·K)) for the dissociation process is attributed to the need to re-organize the solvent dipoles around the charged species[18] formed upon dissociation of **1c**.

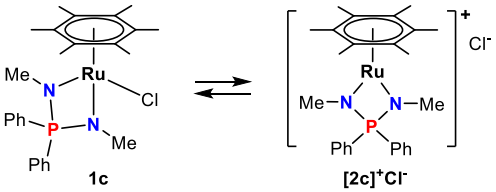

Scheme 2. Chloride dissociation from complex **1c**.

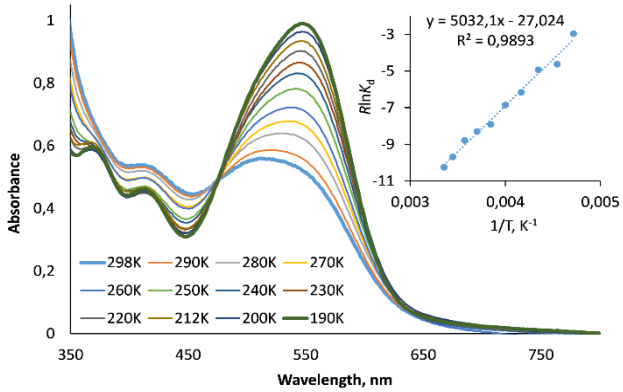

Figure 3. UV-vis spectra of **1c** in CH_2Cl_2 at 190-298 K. The insert shows the Van't Hoff plot of $R\ln K_d$ *vs* 1/T.

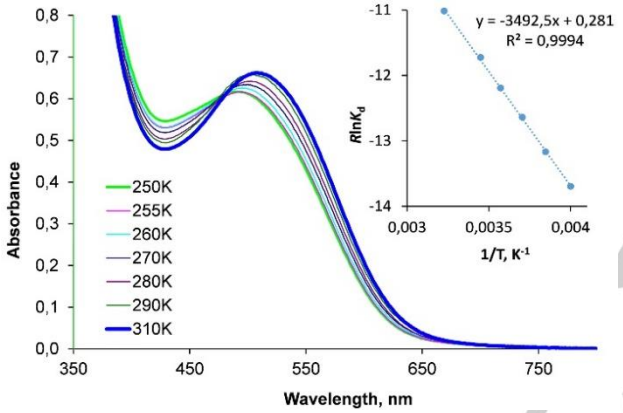

Figure 4. UV-vis spectra of **1b** in $MeNO_2$ at 250-310 K. The insert shows the Van't Hoff plot of $R\ln K_d$ *vs* 1/T.

Complex **1b**, bearing an NPN-ligand with the less electron-releasing *p*-tolyl substituents on the nitrogen atoms, does not show any evidence of chloride dissociation in CH_2Cl_2. The UV-vis spectrum is T-independent and only the undissociated 18ē complexes is present in solution as shown by the band centered at 450 nm (ESI, Fig. S2). However, the compound predominantly exists as cationic complex $[\mathbf{2b}]^+Cl^-$ in solution of the highly polar $MeNO_2$ solvent, exhibiting a band with λ_{max} = 515 nm (Fig. 4). Analysis of the temperature dependence of this band in the range 250-310 K gave ΔH_d = 3.5±0.2 kcal/mol and ΔS_d = +0.3±0.6 cal/(mol·K). Compared to the dissociation of **1c** in CH_2Cl_2, the more positive dissociation entropy of **1b** in $MeNO_2$ is attributed to a more efficient solvation of the charged species by $MeNO_2$. On the other hand, both **1a** and **1d**, which contain the least donating NPN-ligand, do not noticeably dissociate even in $MeNO_2$ as suggested by the absorption band at 450 nm in their visible spectra, even though the insufficient solubility of both compounds did not allow verification of the temperature independence of these spectra.

NMR study of 1a-d in apolar solvents. The chloride complexes **1a-c** show two inequivalent P-Ph groups in their RT-NMR spectra in apolar solvents (benzene, toluene), meaning they exist as C_s-symmetric 18ē complexes on the NMR timescale.[15] We now report that heating the solution of **1c** in C_6D_6 to 338 K gives one set of signals for these groups, which is indicative of exchange. The coalescence of the two *ortho*-protons signals at δ 7.70 and 7.98 is observed at 323±5 K (T_c) (ESI, Fig. S3). From this temperature and from the chemical shift difference, the rate constant (k_{ex} = 380 s^{-1}) and activation free energy ($\Delta G_{ex}^{\neq}$ = 15.2±0.3 kcal/mol) for the degenerative exchange process can be calculated.[19] For complex **1b** with a less donor NPN-ligand, coalescence for the P-Et methyl resonances at δ 0.40 and 1.39 could not be reached below the boiling point of toluene-d_8 (ESI, Fig. S4). However, we observed slow exchange of the ethyl groups for this compound in C_6D_6 and in toluene-d_8 by the 2D EXSY ^{1}H NMR method (Fig. 5),[20] yielding the rate constants of 1.8 s^{-1} and 1.4 s^{-1} at 293 K, respectively (Table 2, lines 3,7). The activation parameters for the exchange process were obtained from the temperature dependence of the exchange rate constants (k_{ex}) in toluene-d_8 in the range 230–315 K: $\Delta H_{ex}^{\neq}$ = 8.4±0.2 kcal/mol and $\Delta S_{ex}^{\neq}$ = -29.2±0.7 cal/(mol·K) (ESI, Fig. S5, Table S1).

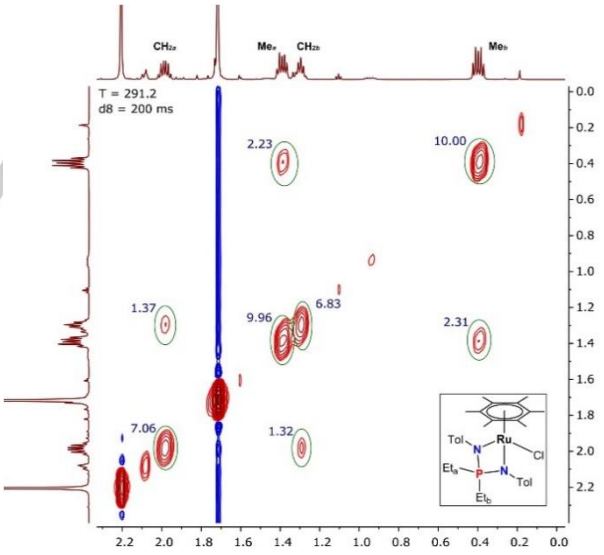

Figure 5. 2D EXSY ^{1}H NMR of **1b** in toluene-d_8 at 291K and the mixing time of 200 ms.

Table 2. Exchange rate constant k_{ex} (s^{-1}) and activation free energy $\Delta G_{ex}^{\neq}$ (kcal/mol) for the P-bound substituent exchange in **1a**, **1b** and **1d** from the 2D EXSY ^{1}H NMR investigations.

	Complex	Solvent	Additives	C(Ru), mM	C(add), mM	*T*, K	k_{ex}, s^{-1}	$\Delta G_{ex}^{\neq}$, kcal/mol
1	**1a**	C_6D_6	-	10		293	<0.1	>18.5
2	**1a**	C_6D_6	H_2O	10	10	294	0.79	17.4
3	**1b**	C_6D_6	-	20		293	1.8	16.8
4	**1b**	C_6D_6	H_2O	20	5	295	>15	<15.7
5	**1b**	Toluene	-	40		295	1.6	17.0
6	**1b**	Toluene	-	8		295	1.6	17.0
7	**1b**	Toluene	-	46		293	1.4	17.0
8	**1d**	C_6D_6		10		293	<0.1	>18.5
9	**1d**	C_6D_6	H_2O	10	0.7	293	0.72	17.3
10	**1d**	C_6D_6	H_2O	10	2.4	293	2.6	16.6
11	**1d**	C_6D_6	$Et_4N^+Cl^-$	10	0.7	292	>11	<15.7

A large negative value of the activation entropy evidences a highly ordered transition state in the exchange process. The exchange between R'$_a$ and R'$_b$ substituents occurs via a configuration inversion at the Ru atom, which can most easily be envisaged by moving the chloride ligand from one coordination side to the opposite one by ligand exchange processes. Generally, such ligand exchange may proceed either via a dissociative mechanism with a cationic 16ē intermediate (pathway **A** in Fig. 6A) or via a S_N2-like associative mechanism through a 20e transition state (pathway **B** in Fig. 6B). In the latter case, however, configuration inversion with exchange of the phosphorus R'$_a$ and R'$_b$ substituents could take place only when the entering ligand is Cl^-. Given that the NMR and UV studies outlined above were carried out in non-coordinating solvents and coordinating ligands L are not present, the exchange in **1b** most likely takes place via the dissociated complex [**2b**]$^+Cl^-$, which requires an entropically unfavorable solvation of the chloride-ion by apolar molecules (Fig. 6A), similarly to the dissociation of **1c** in CH_2Cl_2 described above. We have further confirmed that the exchange rates are independent on the concentration of **1b** (1.6 s^{-1} in both 40 mM and 8 mM toluene-d_8 solutions at 295 K, Table 2, lines 5,6). The P-substituent exchange for complexes **1a** and **1d**, which bear the least electron-donating NPN-ligand, is not observed by 2D EXSY ^{1}H NMR even at t_m = 1 s, hence the rates are slower than 0.1 s^{-1} and the activation free energies ($\Delta G_{ex}^{\neq}$) are greater than 18.5 kcal/mol.

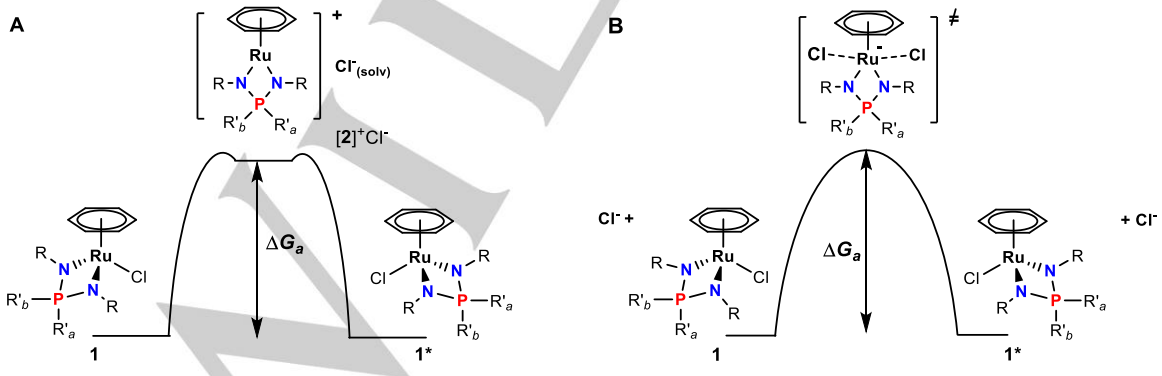

Figure 6. Dissociative (**A**) and associative (**B**) mechanisms for the exchange of the R'$_a$ and R'$_b$ groups in **1**.

In principle, addition of Cl^- should either slow down or accelerate the exchange depending on whether the mechanism is **A** or **B**, respectively. Addition of 0.07 equiv. of $Et_4N^+Cl^-$ to **1d** strongly enhances the exchange process (k_{ex} > 11 s^{-1}). This result strongly suggests that the exchange occurs by the associative mechanism **B** under these conditions (Table 2, line 11, and ESI, Fig. S6). Therefore, it seems that both mechanisms **A** and **B** are possible, the former in the absence of added Cl^- and the latter in its presence.

Assistance by an external ligand L may also result in Cl^- release. While the subsequent attack of the same Ru-L intermediate by Cl^- would not result in any P substituent exchange, attack of another Ru-Cl complex achieves a degenerative self-exchange with configuration inversion and P substituent exchange (Fig. 7). Thus, the P-phenyl group exchange for these compounds becomes observable after adding water to the C_6D_6 solutions (*cf.* lines 1,2 for **1a** and lines 8,9 for **1d**) and the rate constants are found to increase with the increase of the water content (Table 2, lines 9,10; ESI, Fig. S7). For the **1d** sample with [H_2O] = 0.7 mM (0.07 equiv.), the activation parameters could be derived from the temperature dependence (291-335 K) of k_{ex} (ESI, Fig. S8, Table S2). The calculated activation enthalpy[21] $\Delta H_{ex}^{\neq}$ = 11.8±0.2 kcal/mol of the associative exchange can be used as a lower limit for the $\Delta H_{ex}^{\neq}$ in dissociative exchange of **1d** in the absence of external ligands. It is pertinent to underline that water may have a double role in the promotion of the associative chloride exchange: as a ligand to replace Cl^- in the coordination sphere of the Ru atom, and as a proton donor to stabilize the dissociated Cl^- by H-bonding. Interestingly, the effect of water for **1a** is much smaller; a rate constant of 0.79 s^{-1} is achieved only in the presence of an equimolar amount of H_2O in C_6D_6. Perhaps the sterically bulky C_6Me_6 ligand hampers the Cl^- or external ligand coordination thus increasing the activation free energy.

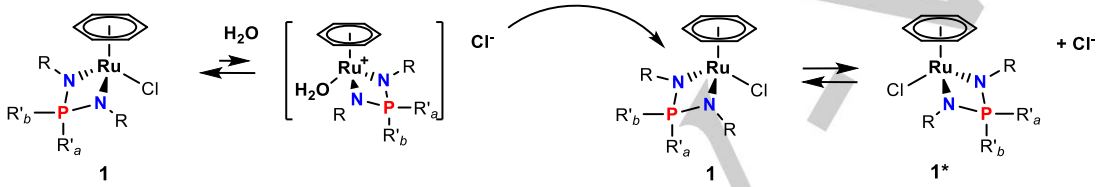

Figure 7. Associative exchange promoted by water-induced chloride dissociation.

We would like to underline that the activation enthalpy $\Delta H_{ex}^{\neq}$ for the exchange process in dissociative mechanism **A** should be very close to the Ru–Cl bond dissociation enthalpy, ΔH_d. The latter depends predominantly on the Ru–Cl bond strength and on the solvent polarity. Hence, the ΔH_d value for complex **1c** may be estimated from its $\Delta G^{\neq}$ at 323 K as $\Delta H_d \sim \Delta H_{ex}^{\neq} = \Delta G_{ex}^{\neq} + T\Delta S_{ex}^{\neq}$, where $\Delta S_{ex}^{\neq}$ can be assumed to be close to that for **1b** (-29.2 cal/(mol·K)). This gives an estimate for the ΔH_d of **1c** as ca. 5.7 kcal/mol. Analogously, the ΔH_d of **1a** and **1d** can be estimated as >10 kcal/mol. Thus, we have proved that the Ru–Cl bond in 18ē arene ruthenium iminophosphonamide complexes can dissociate even in apolar solvents. The ΔH_d for **1a-d** expectedly lowers with an increase of the ligand donating ability: over 10 kcal/mol (**1a**, **1d**) > 8.4 kcal/mol (**1b**) > 5.7 kcal/mol (**1c**).

Coordination of ligands to the 16e cationic complexes 2

We have previously mentioned that the 16ē cationic complex **2a** interacts with MeCN and CO, but failed to isolate these unstable adducts.[15] We have now studied the activity of the 16ē complexes **2** towards coordination of external ligands L (MeCN, pyridine, CO) in detail by means of UV-Vis and NMR spectroscopies (Scheme 3) to determine the thermodynamics of the process and with regard to the conditions allowing isolation. Since **1a** is, among the 18ē chloride complexes **1**, the least prone to chloride dissociation, the corresponding 16ē complex **2a** is expected to display the highest affinity toward saturation by coordination of L ligands. Hence, the coordination of relatively weak donors MeCN and Py was studied for **2a** only.

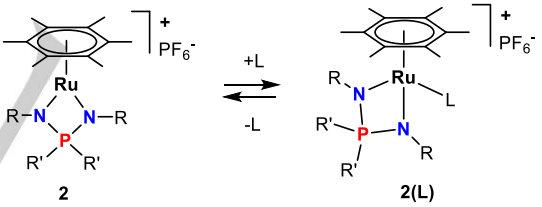

Scheme 3.

The titration of **2a** with MeCN in CH_2Cl_2 at 296 K with UV-Vis monitoring shows that the intensity of the 535 nm band does not significantly change until >100 equiv. of MeCN are added (ESI, Fig. S9A), while a similar amount of pyridine significantly extinguishes this band to give rise a new band of the pyridine adduct at 445 nm (ESI, Fig S9B). The estimated equilibrium constants K_c are <2 M^{-1} for **2a**·MeCN and 32±7 M^{-1} (from UV-vis), 37±1 M^{-1} (from NMR, ESI, Fig. S9C) for **2a**·Py, (ESI, Tables S3-S5). The UV-vis measurements carried out for the 1:2 mixture of **2a**:Py in the temperature range 200-296 K show that **2a** dominates at room temperature, while the equilibrium shifts towards formation of the 18ē adduct **2a**·**Py** at lower temperatures. The conversion becomes essentially complete below 220 K (Fig. 8). The analysis of the Van't Hoff's plot yields ΔH_c = -12.4±0.5 kcal/mol and ΔS_c = -36±2 cal/(mol·K). Thus, pyridine coordination is moderately exothermic, but a large excess of pyridine is

required to observe coordination at room temperature because of high association entropy. This is in sharp contrast with the previously reported irreversible coordination of pyridine to the 16ē arene ruthenium amidinate complex [(C_6H_6)Ru(^{t}BuN-C(Ph)-N^{t}Bu}](BAr$^F_4$).[10]

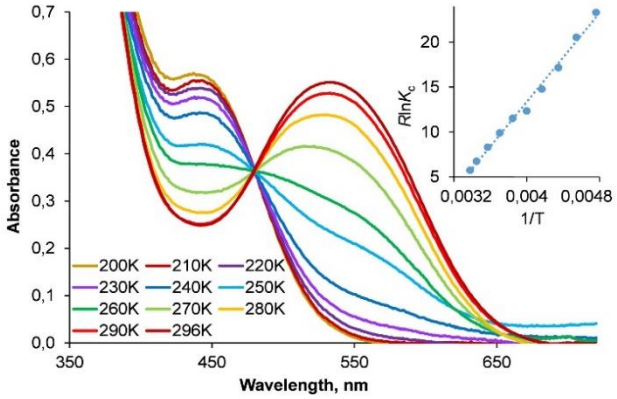

Figure 8. UV-vis spectra of reversible coordination of pyridine to **2a** in CH_2Cl_2 at 200-296K. The insert shows the Van't Hoff dependence of $R\ln K_c$ *vs* 1/T.

In comparison with acetonitrile and pyridine, carbon monoxide is a stronger π-acceptor and reacts readily with **2a** to give the CO adduct **3a**. However, the reaction is reversible and facile CO decoordination occurs upon solvent evaporation to give back **2a**. Nevertheless, **3a** could be isolated by precipitation from its CH_2Cl_2 solution upon addition of excess diethyl ether. Analogously, the reaction of **2d** with CO resulted in formation of **3d**, which is stable only under a CO atmosphere. This product was isolated, like **3a**, by using CO-saturated CH_2Cl_2 solution and diethyl ether. Although **3a** and **3d** slowly evolve CO in the solid state under vacuum, satisfactory elemental analyses were obtained for both. It should be noted that **3a** is stable in a CO-saturated solution, whereas **3d** degrades within days to unknown arene-free carbonyl complexes, perhaps similar to the previously observed ones resulting from the decomposition of [(*p*-Cymene)Ru(CO)(SXyl)$_2$].[22] The molecular structures of **3a,d** were determined by single crystal X-ray diffraction (ESI, Table S6). Selected structural parameters and views of the molecules are shown in Figures 9 and 10.

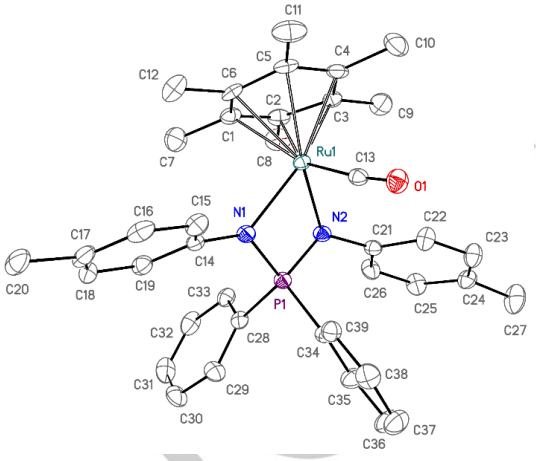

Figure 9. ORTEP diagram of the cation **3a**. Ellipsoids are shown at the 50% probability level. The hydrogen atoms and the anion are omitted for clarity. Selected bond lengths (Å) and angles (°): Ru···Arene(centroid) 1.769(1), Ru–C(O) 1.871(3), Ru–N1 2.112(2), Ru–N2 2.116(2), C–O 1.145(3), N1–Ru–N2 69.20(9), Ru–N1–P–N2 164.60(15), Σ(N1) 348.3(5), Σ(N2) 359.3(5).

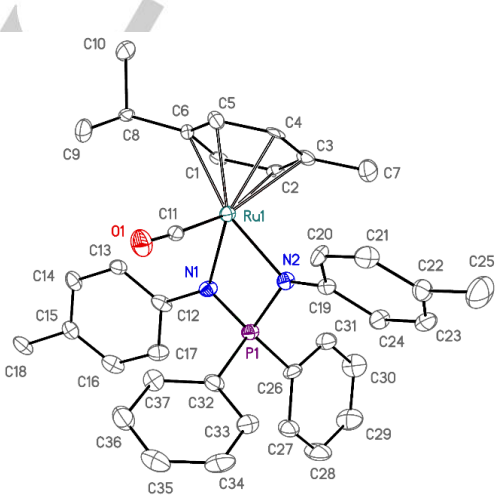

Figure 10. ORTEP diagram of the cation **3d**. Ellipsoids are shown at the 50% probability level. The hydrogen atoms and the anion are omitted for clarity. Selected averaged bond lengths (Å) and angles (°): Ru···Arene(centroid) 1.768(3), Ru–C(O) 1.879(9), Ru–N1 2.095(7), Ru–N2 2.120(6), C–O 1.145(10), N1–Ru–N2 68.9(3), Ru–N1–P–N2 165.8(4), Σ(N1) 353.7(13), Σ(N2) 355.3(14).

Complexes **3a** and **3d** are the first crystallographically characterized arene ruthenium carbonyl derivatives with any κ^2-N,N-anionic chelate ligand. The asymmetric unit of **3d** contains two independent molecules, which exhibit identical metric parameters within experimental error. Both complexes exhibit a three-legged piano stool geometry with a pseudo octahedral configuration of the ligands around the ruthenium atom. The coordinated arene adopts a nearly staggered (**3a**) or eclipsed (**3d**) conformation relative to the Ru-CO axis, with C4–Arene(centroid)–Ru–CO angles of 25.7° and 5.9–6.4°, respectively. The presence of the CO ligand significantly increases the Ru–Arene(centroid) distance by ~0.1 Å in both **3a** and **3d** relative to **2a** (1.662(2) Å) and **2d**. The Ru–C(arene)

distances vary in the range 2.208–2.333(3) Å with the longest bonds being *trans* to the CO ligand. The C–C bonds length (1.389(12)–1.452(4) Å) in the coordinated arene slightly alternate with the shortest C–C bond (1.389–1.403 Å) located *trans* to the CO ligand. A similar Ru–Arene(centroid) (1.810 Å), Ru–C(O) (1.846(4) Å) and carbonyl C–O (1.133(7) Å) distances, as well as elongations for the two Ru–C(arene) bonds *trans* to CO (2.389–2.396 Å) were previously reported for the arene ruthenium dithiolate carbonyl complex [(η^6-C_6Me_6)Ru(CO)($S_2C_6H_4$)] (**4**).[17] The Ru–N bonds are shorter than those in the neutral 18ē complexes **1a-d** by ca. 0.04 Å, reflecting the presence of the positive charge, but longer (by 0.05-0.08 Å) than in the 16ē complexes **2a-d**, in which they are strengthened by π-donation from the NPN-ligand. The chelate N1–Ru–N2 angles in **3a** and **3d** are similar to those of the other 18ē NPN-complexes **1a-d**. However, unlike in the related chloride complexes **1a** and **1d**, the Ru–N1–P–N2 metallacycles in **3a** and **3d** are folded by 13–15.6° from planarity at the N1···N2 hinge and the nitrogen atoms (N1 in **3a**; N1 and N2 in **3d**) are noticeably pyramidalized as shown by the Σ(N) parameter. There are several close H···F contacts between the cation and the PF_6^- anion in both structures, although none of these is shorter than the sum of the van der Waals radii of H and F (2.56 Å).[23]

Complexes **3a** and **3d** are sufficiently stable in concentrated solutions to allow recording their NMR spectra, although the fraction of the corresponding 16ē complexes increases with time. The ^{31}P NMR resonance (δ 61.7 for **3a** and δ 60.2 for **3d**) is downfield shifted by *ca*. 10 ppm relative to the corresponding 16ē cationic complexes **2a** and **2d**. In the ^{1}H and ^{13}C{^{1}H} NMR spectra recorded in $CDCl_3$ there are two sets of signals for the magnetically inequivalent phenyl groups at the phosphorus atom, as expected for the C_s-symmetric complexes, hence the decoordination of CO is a slow process with a relatively high activation barrier. The resonance of the coordinated CO ligand in the ^{13}C NMR spectra is observed at high field (δ 199.2, 193.8), as is typical of terminal linear coordinated CO ligands (cf. to δ 197.8 for **4**[17] and δ 203-208 reported for the cyclopentadienyl ruthenium complexes with N,N-ligands).[9, 24]

Both carbonyl adducts **3a** and **3d** exhibit strong CO stretching vibration band in the IR spectrum at 1984 cm^{-1} (**3a**) and 2012 cm^{-1} (**3d**). The higher ν_{CO} in **3d** evidences weaker Ru-CO π-back-bonding relative to **3a** that possesses the electron-richer C_6Me_6 arene. These frequencies are substantially lower than those of the more electron-deficient arene ruthenium amidinate carbonylic complex [(η^6-C_6H_6)Ru(CO){PhC(N^{t}Bu)$_2$}](BAr$^F_4$) (ν_{CO} = 2050 cm^{-1}),[10] but closer to those of the arene ruthenium complex with dianionic ditiolate ligands **4** (ν_{CO} = 1951 cm^{-1}),[17] [(η^6-C_6Me_6)Ru(CO)(SXyl)$_2$] (ν_{CO} = 1965 cm^{-1})[22] and of the cyclopentadienyl complex with neutral κ^2-N,N-ligand [(η^5-C_5H_5)Ru(CO)(TMEDA)](BAr$_4$) (ν_{CO} = 1968 cm^{-1}).[24]

Surprisingly, bubbling CO into the solution of **2c** yielded a stable product, **3c**, resulting from the addition of two CO molecules, one of which has inserted into one of the two Ru–N bonds. The product has been fully characterized, including by single crystal X-ray diffractometry (Figure 11, Table S6 in ESI).

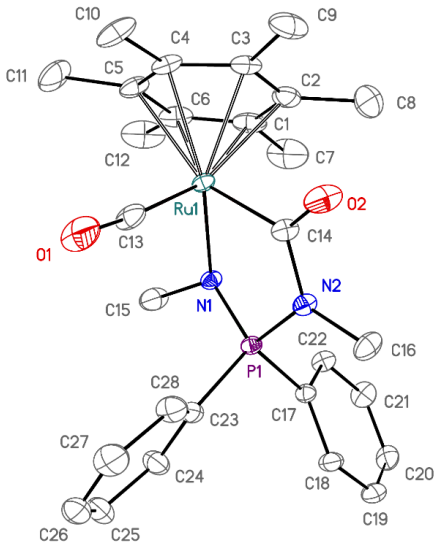

Figure 11. ORTEP diagram of the cation **3c**. Ellipsoids are shown at 30% probability level. The hydrogen atoms and the anion are omitted for clarity. Selected bond lengths (Å) and angles (°): Ru···Arene(centroid) 1.828(1), Ru–N1 2.107(2), Ru–C(O)N 2.042(3), C=O 1.211(4), N–C(O) 1.414(3), Ru–C(O) 1.859(3), C–O 1.143(4), N1–Ru–C(O) 83.15(10), Σ(N1) 349.7(5), Σ(N2) 359.3(6).

The overall geometry of **3c** is similar to that of **3a,d** except for the expanded metallacycle with a CO group. The addition of two CO molecules leads to a significant increase of the Ru–Arene(centroid) distance relative to **2c** by *ca*. 0.18 Å as a result of elongation of the Ru–C(arene) bonds *trans* to the terminal CO (2.299–2.312(3) Å) and to the carbamoyl C=O group (2.373–2.381(3) Å). The arene C–C bonds *trans* to the terminal CO (1.404(6) Å) and to C=O group (1.392(5) Å) are shorter than the other four bonds (1.417–1.438(5) Å). Similarly to **3a** and **3d**, the terminal carbonyl group is linear. The carbamoyl C=O and C–N bonds have similar length to or are slightly longer than those in organic amides. The carbamoyl N2 atom is planar, while N1 is considerably pyramidalized as in the corresponding 18ē chloride complex **1c**. There are two intermolecular close contacts in the structure of **3c** that fall below the sum of the van der Waals radii,[23] implicating hydrogen atoms of the C_6Me_6 ligand and either a PF_6^- F atom or the carbamoyl oxygen atom, H(8A)···F (2.269 Å) and H(10B)···O(2)C (2.418 Å), respectively.

The ^{13}C{^{1}H} NMR spectrum of **3c** reveals two signals corresponding to carbonyl C nuclei: a singlet at δ 198.2 and a doublet at δ 192.8 ($^2J_{CP}$ = 19.6 Hz). All the N- and P-substituents in **3c** are inequivalent and give rise to two sets of signals for both methyl and phenyl groups in the ^{1}H and ^{13}C{^{1}H} spectra. In the IR spectra **3c** shows two strong carbonyl bands ν_{CO} at 1984 cm^{-1} (metal bound CO) and at 1644 cm^{-1} (carbamoyl C=O), the latter frequency being typical of organic amides.

Apparently, the carbonylation of **2c** is a two-step reaction involving: 1) coordination of a first CO molecule to give an intermediate **C**, which is structurally similar to **3a,d**; and 2)

insertion of the terminal CO into a Ru–N bond and subsequent occupation of the resulting vacant site at the ruthenium atom by a second CO molecule (Scheme 4). This conclusion is further supported by the results of an IR spectroscopic monitoring at low temperatures (Fig. 12). Bubbling CO at -40°C for 10 s fully converts **2c** to an orange complex characterized by a strong CO band at 1975 cm^{-1}, which can be attributed to the mono-adduct **C**. The latter is unstable: even at -40°C and in the absence of additional CO it slowly disappears to be replaced by **3c**. The coordination of the first CO molecule is reversible, hence dissociation from the mono-adduct **C** provides the needed CO for the second carbonylation step. The rearrangement is complete within a few minutes at low temperatures and yields a 1:1 mixture of **2c** and **3c**, which were isolated upon evaporation of the solvent.

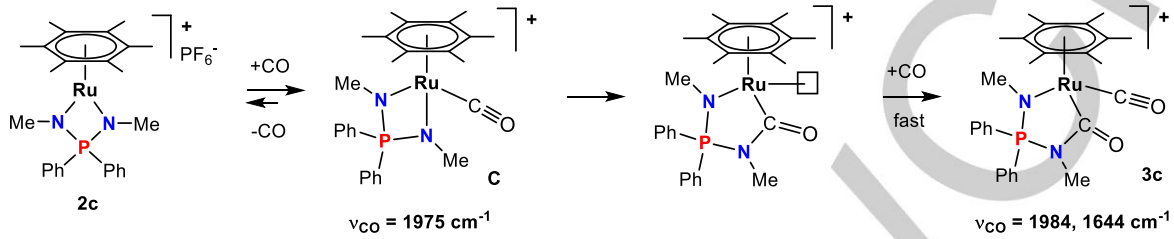

Scheme 4.

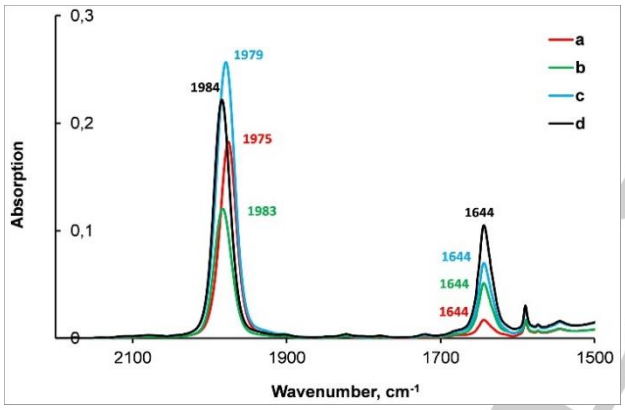

Figure 12. The reaction of **2c** with CO monitored by IR. The sample was dissolved in CH_2Cl_2 at -40°C and CO was bubbled for 10 s. The spectra were recorded (a) immediately after the preparation, (b) after 40 s at room temperature, (c) after 5 min of keeping (a) at -40°C, (d) after evaporation of (c) and redissolution in CH_2Cl_2.

The peculiarity of the mono-carbonyl intermediate **C** is the high nucleophilicity of the nitrogen atoms, which is related to the presence of more electron-donating alkyl substituents. Although facile CO-insertion into M–N bonds is a known phenomenon for certain metal aminopyridinates,[25] triazenides,[26] amidinates,[27-30] and aminophosphines[31] this reaction has not been previously reported to the best of our knowledge for arene ruthenium complexes. The process that most resembles the formation of **3c** involves a carbene insertion into a Ru–N bond in the arene ruthenium amidinate complex $[(C_6Me_6)Ru\{(^iPrN)_2CMe\}](PF_6)$, followed by CO coordination to give $[(C_6Me_6)Ru(CO)\{(^iPrN)$-$CMe(N^iPr)CHSiMe_3\}](PF_6)$ (**5**).[32] The spectral and structural data of **5** are similar to those of **3c**: the ν_{CO} is observed at 1963 cm^{-1} and the carbonyl resonance appears at δ 203 in the ^{13}C NMR spectrum; the Ru–Arene(centroid) distance is 1.828 Å with the elongation of the Ru–C(arene) bonds *trans* to CO and to the inserted carbene to 2.320–2.362 Å; the CO ligand is linear (Ru–C–O is 170.2°), and the Ru–CO and C–O bond lengths are 1.836 Å and 1.159 Å, respectively.

Conclusions

Our detailed spectroscopic study has allowed to investigate the stabilization of the coordinative unsaturation in half-sandwich ruthenium iminophosphonamide complexes depending on the N-,P-substituents, arene and other co-ligands. By 2D EXSY ^1H NMR spectroscopy we have proven that the dynamic exchange process observed for chlorides **1a-d** is attributed to the dissociation of the chloride ligand via a 16ē intermediate in both polar and apolar solvents. The chloride dissociation enthalpy (ΔH_d) determined for the 18ē chloride complexes **1a-d** and the Cl^- coordination enthalpy (ΔH_c) to the 16ē complex **2a** quantitatively estimate the stabilization effect of the NPN ligand, which is mostly provided by highly localized negative charges at the nitrogen atoms via additional π-donation. Hence the NPN ligands with N-alkyl groups destabilize the 18ē complexes and compensate the metal electron deficiency much more effectively than the NPN ligands with N-aryl groups. Thus, the N-Me chloride complex **1c** dissociates exothermically (ΔH_d = -5.0 kcal/mol) even in CH_2Cl_2, whereas the dissociation is always endothermic for the N-Tol complexes (**1a**, **1b** and **2d**), even in polar nitromethane. On the other hand, the less donating arene ligand (*p*-cymene *vs* C_6Me_6) affects the stability of the 18ē complexes counterintuitively: it destabilizes the carbonyl adducts due to the lack of electron density provided for π-backdonation (**3d** *vs* **3a**), but enhances the stability of the chloride complex (**1d** *vs* **1a**) due to lower energy of the orbital corresponding to Ru-Cl bond. The coordination of ligands to 16ē complexes **2** appears to be unambiguously exothermic, while the highly negative association entropy makes the 18ē complexes stable only at low temperatures. Nevertheless, stronger π-acceptors (CO > pyridine > MeCN) give more stable adducts due to significant contribution of π-backdonation to Ru-L bonding; this fact allowed us to isolate and structurally

characterize complexes **3a** and **3d**, which are rare examples of cationic 18ē arene ruthenium carbonyl complexes. The unexpectedly facile insertion of CO into the Ru–N bond observed in the 18ē adduct **2c**·CO to give the carbonyl-carbamoyl complex **3c** proves that arene ruthenium iminophosphonamide complexes can react in diverse manners and suggests that they have potential for application in organic synthesis and (bifunctional) catalysis. Further investigation of these complexes in catalytic transfer hydrogenation is in progress and will be reported soon.

Experimental Section

General procedures. All manipulations were carried out using standard Schlenk techniques under an atmosphere of dry argon. Absolute solvents were used for both synthesis and spectroscopic studies; solvents were purified by standard methods and distilled prior to use. The ^{1}H, ^{31}P and ^{13}C NMR spectra were obtained on Bruker Avance 600 or Bruker Avance 400 spectrometers and referenced to the residual signals of deuterated solvent (^{1}H and ^{13}C), and to 85% H_3PO_4 (^{31}P, external standard). The UV spectra were recorded on a Varian Cary 50 WinUV spectrometer in quartz cells (*l* = 2.2 mm or 10 mm). The IR spectra were obtained on a Fourier spectrometer Nicolet 6700 in KBr cells (*l* = 0.514 mm). The elemental analyses were carried out on a Carlo Erba 1106 CHN analyzer. The following compounds were prepared according to described procedures: [(η^6-*p*-Cymene)$RuCl_2$]$_2$,[33] Ph_2P(N-*p*-Tol)(NH-*p*-Tol) (**A**),[15] **1a-c**, **2a-c**.[15]

Synthesis of [(η^6-*p*-Cymene)RuCl{Ph_2P(N-*p*-Tol)$_2$}] (1d). To a solution of **A** (0.79 g, 2.00 mmol) in benzene (60 mL) a 2.0 M solution of NaHMDS in THF (1.10 mL, 2.20 mmol) was added and the resulting solution was stirred for 2 h. Then solid [(η^6-*p*-Cymene)$RuCl_2$]$_2$ (0.61 g, 1.00 mmol) was added and the reaction mixture was stirred overnight. The reaction mixture was filtered and the solvent from the filtrate was removed under reduced pressure. The residue was washed with hexane (2x10 mL), Et_2O (2x5 mL), and then recrystallized from hot benzene (20 ml). The dark-red crystalline was filtered off, washed with Et_2O (5 mL) and dried *in vacuo*. Yield 1.00 g (88%). Anal. calcd for $C_{36}H_{38}ClN_2PRu$: C, 64.90; H, 5.75%. Found: C, 64.85; H, 5.84%. ^{31}P NMR ($CDCl_3$): δ 43.8 (s, PPh_2). ^{1}H NMR ($CDCl_3$): δ 7.87 (dd, $^{3}J_{HP}$ = 10.8, $^{3}J_{HH}$ = 8.0, 4H, *o*-H_{Ph}), 7.50 (m, 2H, *p*-H_{Ph}), 7.39 (m, 4H, *m*-H_{Ph}), 6.90 (d, $^{3}J_{HH}$ = 8.0, 4H, C_6H_4(Tol)), 6.82 (d, $^{3}J_{HH}$ = 8.4, 4H, C_6H_4(Tol)), 6.31 (d, $^{3}J_{HH}$ = 5.6, 2H, C_6H_4(Cym)), 5.41 (d, $^{3}J_{HH}$ = 5.6, 2H, C_6H_4(Cym)), 2.89 (sept, $^{3}J_{HH}$ = 6.8, 1H, *CH*Me_2), 2.19 (s, 6H, Me_{Tol}), 2.11 (s, 3H, Me_{Cym}), 1.21 (d, $^{3}J_{HH}$ = 6.8, 6H, CH*Me*$_2$). ^{31}P NMR (C_6D_6): δ 42.9. ^{1}H NMR (C_6D_6): δ 8.03 (m, 4H, *o*-H_{Ph}), 7.27 (d, $^{3}J_{HH}$ = 7.8, 4H, C_6H_4(Tol)), 7.22 (m, 3H, *(m+p)*-H_{Ph}), 6.93 (d, $^{3}J_{HH}$ = 7.8, 4H, C_6H_4(Tol)), 6.75 (m, 3H, *(m+p)*-$H_{Ph'}$), 5.05 (d, $^{3}J_{HH}$ = 6.0, 2H, C_6H_4(Cym)), 4.87 (d, $^{3}J_{HH}$ = 6.0, 2H, C_6H_4(Cym)), 2.88 (sept, $^{3}J_{HH}$ = 6.6, 1H, *CH*Me_2), 2.15 (s, 6H, Me_{Tol}), 1.86 (s, 3H, Me_{Cym}), 1.05 (d, $^{3}J_{HH}$ = 6.8, 6H, CH*Me*$_2$). ^{13}C NMR ($CDCl_3$): δ 145.8 (d, $^{2}J_{CP}$ = 4.4, *i*-C_{Tol}(N)), 133.4 (br.s, *o*-C_{Ph}), 131.9 (d, $^{4}J_{CP}$ = 2.7, *p*-C_{Ph}), 129.0 (s, β-CH_{Tol}), 128.2 (d, $^{3}J_{CP}$ = 11.2, *m*-C_{Ph}), 127.5 (s, *i*-C_{Tol}(Me)), 122.9 (d, $^{3}J_{CP}$ = 9.7, α-CH_{Tol}), 102.0 (s, *i*-C_{Cym}), 94.8 (s, *i*-C_{Cym}), 80.5 (s, CH_{Cym}), 79.6 (s, CH_{Cym}), 30.9 (s, *CH*Me_2), 22.5 (s, CH*Me*$_2$), 20.5 (s, Me_{Tol}), 18.9 (s, Me_{Cym}). ^{13}C NMR (C_6D_6): δ 146.9 (s, $^{2}J_{CP}$ = 4.2, *i*-C_{Tol}(N)), 136.5 (d, $^{1}J_{CP}$ = 95.1, *i*-C_{Ph}), 135.0 (d, $^{2}J_{CP}$ = 11.0, *o*-C_{Ph}), 132.6 (d, $^{2}J_{CP}$ = 9.8, *o*-$C_{Ph'}$), 132.0 (d, $^{4}J_{CP}$ = 2.7, *p*-C_{Ph}), 131.8 (d, $^{4}J_{CP}$ = 2.9, *p*-$C_{Ph'}$), 130.2 (d, $^{1}J_{CP}$ = 84.0, *i*-$C_{Ph'}$), 129.4 (s, β-CH_{Tol}), 128.6 (d, $^{3}J_{CP}$ = 12.5, *m*-C_{Ph}), 128.5 (s, *i*-C_{Tol}(Me)), ~127.7 (overlapped, *m*-$C_{Ph'}$), 123.9 (d, $^{3}J_{CP}$ = 9.7, α-CH_{Tol}), 102.4 (s, *i*-C_{Cym}), 94.8 (s, *i*-C_{Cym}), 80.7 (s, CH_{Cym}), 79.4 (s, CH_{Cym}), 31.2 (s, *CH*Me_2), 22.5 (s, CH*Me*$_2$), 20.7 (s, Me_{Tol}), 18.8 (s, Me_{Cym}). UV-vis (CH_2Cl_2; λ_{max}, nm; ε, M^{-1} cm^{-1}): 450 (450, shoulder).

Synthesis of [(η^6-*p*-Cymene)Ru{Ph_2P(N-*p*-Tol)$_2$}](PF_6) (2d). To a solution of **1d** (0.39 g, 0.59 mmol) in CH_2Cl_2 (15 ml), solid $AgPF_6$ (0.16 g, 0.62 mmol) was added, causing the color to immediately change from red to deep violet. The reaction mixture was stirred for 2 h and then filtered through a bed of Celite. The solvent was removed under reduced pressure, and the residue was dried *in vacuo* to give violet-black **2d**. Yield 0.41 g (91%). Anal. calcd for $C_{36}H_{38}F_6N_2P_2Ru$: C, 55.74; H, 4.94%. Found: C, 55.47; H, 4.99%. ^{31}P NMR ($CDCl_3$): δ 71.3 (s, PPh_2), -144.1 (sept, J_{PF} = 712, PF_6^-). ^{1}H NMR ($CDCl_3$): δ 7.65 (m, 2H, *p*-H_{Ph}), 7.52 (m, 4H, *m*-H_{Ph}), 7.47 (m, 4H, *o*-H_{Ph}), 7.02 (d, $^{3}J_{HH}$ = 8.0, 4H, C_6H_4), 6.84 (dd, $^{3}J_{HH}$ = 8.0, $^{4}J_{HP}$ = 1.2, 4H, C_6H_4), 5.88 (d, $^{3}J_{HH}$ = 6.8, 2H, C_6H_4(Cym)), 5.84 (d, $^{3}J_{HH}$ = 6.8, 2H, C_6H_4(Cym)), 2.68 (sept, $^{3}J_{HH}$ = 6.8, 1H, *CH*Me_2), 2.26 (s, 3H, Me_{Cym}), 2.25 (s, 6H, Me_{Tol}), 1.31 (d, $^{3}J_{HH}$ = 6.8, 6H, CH*Me*$_2$). ^{13}C NMR ($CDCl_3$): δ 144.1 (d, $^{2}J_{CP}$ = 3.6, *i*-C_{Tol}(N)), 134.4 (d, $^{4}J_{CP}$ = 2.2, *p*-C_{Ph}), 134.1 (s, *i*-C_{Tol}(Me)), 132.4 (d, $^{2}J_{CP}$ = 10.3, *o*-C_{Ph}), 130.2 (s, β-CH_{Tol}), 129.5 (d, $^{3}J_{CP}$ = 12.5, *m*-C_{Ph}), 124.7 (d, $^{1}J_{CP}$ = 89.4, *i*-C_{Ph}), 123.7 (d, $^{3}J_{CP}$ = 8.0, α-CH_{Tol}), 99.6 (s, *i*-C_{Cym}), 89.6 (s, *i*-C_{Cym}), 81.0 (s, CH_{Cym}), 78.7 (s, CH_{Cym}), 31.8 (s, *CH*Me_2), 22.8 (s, CH*Me*$_2$), 20.9 (s, Me_{Tol}), 19.7 (s, $\underline{Me}_{Cym}$). UV-vis (CH_2Cl_2; λ_{max}, nm; ε, M^{-1} cm^{-1}): 590 (1880).

Reaction of 2a,2c,2d with CO. General procedure. A stream of CO was slowly bubbled through a stirred solution of **2a** (0.12 g, 0.15 mmol) in CH_2Cl_2 (5 mL) for 10 min. The color quickly changed from deep violet to orange. The product was precipitated with Et_2O (20 ml) as a yellow-orange crystalline solid, which was filtered off and dried *in vacuo* for 1 hr. Yield 0.12 g (96%). Anal. calcd for $C_{39}H_{42}F_6N_2OP_2Ru$: C, 56.32; H, 5.09%. Found: C, 56.34; H, 4.95%. ^{31}P NMR (CD_2Cl_2): δ 61.7 (s, PPh_2), -144.5 (sept, $^{1}J_{PF}$ = 713, PF_6^-). ^{1}H NMR (CD_2Cl_2): δ 7.84 (t, $^{3}J_{HH}$ = 8.6, 1H, *p*-H_{Ph}), 7.81 (dd, $^{3}J_{HP}$ = 12.8, $^{3}J_{HH}$ = 8.0, 2H, *o*-H_{Ph}), 7.69 (dt, $^{3}J_{HH}$ = 7.2, $^{4}J_{HP}$ = 3.2, 2H, *m*-H_{Ph}), 7.48 (dt, $^{3}J_{HH}$ = 7.2, $^{5}J_{HP}$ = 1.6, 1H, *p*-$H_{Ph'}$), 7.24 (dt, $^{3}J_{HH}$ = 8.0, $^{4}J_{HP}$ = 3.2, 2H, *m*-$H_{Ph'}$), 7.19 (dd, $^{3}J_{HP}$ = 10.8, $^{3}J_{HH}$ = 8.0, 2H, *o*-$H_{Ph'}$), 6.90 (d, $^{3}J_{HH}$ = 8.0, 4H, C_6H_4(Tol)), 6.46 (dd, $^{3}J_{HH}$ = 8.0, $^{4}J_{HP}$ = 2.0, 4H, C_6H_4(Tol)), 2.21 (s, 6H, Me_{Tol}), 2.11 (s, 18H, C_6Me_6). ^{13}C NMR (CD_2Cl_2): δ 199.2 (s, Ru-CO), 140.8 (d, $^{2}J_{CP}$ = 2.2, *i*-C_{Tol}(N)), 135.8 (d, $^{1}J_{CP}$ = 97.2, *i*-C_{Ph}), 134.9 (d, $^{4}J_{CP}$ = 2.6, *p*-C_{Ph}), 133.6 (d, $^{4}J_{CP}$ = 2.7, *p*-$C_{Ph'}$), 132.9 (d, $^{2}J_{CP}$ = 9.3, *o*-C_{Ph}), 132.7 (d, $^{2}J_{CP}$ = 11.0, *o*-$C_{Ph'}$), 132.8 (s, *i*-C_{Tol}(Me)), 130.4 (d, $^{4}J_{CP}$ = 1.3, β-CH_{Tol}), 130.0 (d, $^{3}J_{CP}$ = 12.1, *m*-C_{Ph}), 128.9 (d, $^{3}J_{CP}$ = 11.4, *m*-$C_{Ph'}$), 128.3 (d, $^{1}J_{CP}$ = 83.3, *i*-$C_{Ph'}$), 126.0 (d, $^{3}J_{CP}$ = 7.0, α-CH_{Tol}), 110.3 (s, C_6Me_6), 20.8 (s, Me_{Tol}), 17.1 (s, $C_6\underline{Me}_6$). UV-vis (CH_2Cl_2; λ_{max}, nm; ε, M^{-1} cm^{-1}): 450 (100, shoulder). IR (CH_2Cl_2, *v*, cm^{-1}): 1984 (RuCO).

Analogously, from **2c** (0.10 g, 0.15 mmol) in CH_2Cl_2 (3 ml), complex **3c** was obtained as a stable yellow crystalline solid. Yield 0.10 g (95%). Anal. calcd for $C_{28}H_{34}F_6N_2O_2P_2Ru$•$H_2O$: C, 46.35; H, 5.00%. Found: C, 46.49; H, 5.00%. ^{31}P NMR (CD_2Cl_2): δ 55.2 (s, PPh_2), -144.5 (sept, $^{1}J_{PF}$ = 713, PF_6^-). ^{1}H NMR (CD_2Cl_2): δ 7.83 (ttd, $^{3}J_{HH}$ = 7.8, $^{4}J_{HH}$ = 1.8, $^{5}J_{HP}$ = 1.2, 1H, *p*-H_{Ph}), 7.75 (ttd, $^{3}J_{HH}$ = 7.8, $^{4}J_{HH}$ = 1.2, $^{5}J_{HP}$ = 1.2, 1H, *p*-$H_{Ph'}$), 7.71 (dt, $^{3}J_{HH}$ = 7.8, $^{4}J_{HP}$ = 3.6, 2H, *m*-H_{Ph}), 7.63 (ddd, $^{3}J_{HP}$ = 12.6, $^{3}J_{HH}$ = 7.8, $^{4}J_{HH}$ = 1.2, 2H, *o*-H_{Ph}), 7.60 (dt, $^{3}J_{HH}$ = 7.8, $^{4}J_{HP}$ = 3.6, 2H, *m*-$H_{Ph'}$), 7.42 (ddd, $^{3}J_{HP}$ = 12.6, $^{3}J_{HH}$ = 7.8, $^{4}J_{HH}$ = 1.2, 2H, *o*-$H_{Ph'}$), 2.73 (d, $^{3}J_{HP}$ = 8.4, 3H, N*Me*(CO)), 2.64 (d, $^{3}J_{HP}$ = 17.4, 3H, NMe), 2.24 (s, 18H, C_6Me_6). ^{13}C NMR (CD_2Cl_2): δ 198.2 (s, Ru-CO), 192.8 (d, $^{2}J_{CP}$ = 19.6, NC=O), 135.1 (d, $^{4}J_{CP}$ = 2.4, *p*-C_{Ph}), 135.0 (d, $^{4}J_{CP}$ = 2.4, *p*-$C_{Ph'}$), 133.6 (d, $^{2}J_{CP}$ = 10.6, *o*-$C_{Ph'}$), 132.6 (d, $^{2}J_{CP}$ = 10.6, *o*-C_{Ph}), 130.3 (d, $^{3}J_{CP}$ = 12.8, *m*-C_{Ph}), 130.2 (d, $^{3}J_{CP}$ = 12.6, *m*-$C_{Ph'}$), 124.2 (d, $^{1}J_{CP}$ = 112.2, *i*-C_{Ph}), 122.2 (d, $^{1}J_{CP}$ = 98.6, *i*-$C_{Ph'}$), 113.4 (s, *i*-C_6Me_6), 39.3 (d, $^{3}J_{CP}$ = 4.2, NMe), 29.3 (d, $^{3}J_{CP}$ = 8.4, N*Me*(CO)), 17.0 (s, C_6Me_6),. IR (CH_2Cl_2, v, cm^{-1}): 1983 (RuCO), 1644 (RuC(O)N).

Analogously, carbonylation of **2d** (0.11 g, 0.14 mmol) gave a red solution of **3d**. The product was precipitated by Et_2O (20 ml) saturated with CO, filtered and dried *in vacuo* for 30 min. Yield 0.09 g (82%). Anal. calcd for $C_{37}H_{38}F_6N_2OP_2Ru$: C, 55.29; H, 4.77%. Found: C, 55.05; H, 4.86%. ^{31}P NMR ($CDCl_3$): δ 60.2 (s, PPh_2), -144.2 (sept, $^{1}J_{PF}$ = 713, PF_6^-). ^{1}H NMR ($CDCl_3$): δ 7.93 (dd, $^{3}J_{HP}$ = 12.4, $^{3}J_{HP}$ = 7.2 , 2H, *o*-H_{Ph}), 7.80 (t, $^{3}J_{HH}$ = 7.2,

1H, *p*-H_{Ph}), 7.73 (dt, $^3J_{HH}$ = 7.6, $^4J_{HP}$ = 2.8, 2H, *m*-H_{Ph}), 7.50 (t, $^3J_{HH}$ = 7.2, 1H, *p*-$H_{Ph'}$), 7.35 (dd, $^3J_{HP}$ = 10.2, $^3J_{HH}$ = 7.2, 2H, *o*-$H_{Ph'}$), 7.30 (dt, $^3J_{HH}$ = 7.6, $^3J_{HH}$ = 3.2, 2H, m-$H_{Ph'}$), 6.87 (d, $^3J_{HH}$ = 8.0, 4H, C_6H_4(Tol)), 6.51 (d, $^3J_{HH}$ = 8.0, 4H, C_6H_4(Tol)), 6.29 (br. s, 4H, C_6H_4(Cym)), 2.65 (sept, $^3J_{HH}$ = 6.8, 1H, *CH*Me_2), 2.18 (s, 6H, Me_{Tol}), 2.11 (s, 3H, Me_{Cym}), 1.22 (d, $^3J_{HH}$ = 6.8, 6H, CH*Me*$_2$). ^{13}C NMR ($CDCl_3$): δ 193.8 (s, Ru-CO), 143.1 (d, $^2J_{CP}$ = 3.4, *i*-C_{Tol}(N)), 134.5 (d, $^4J_{CP}$ = 2.6, *p*-C_{Ph}), 133.7 (d, $^4J_{CP}$ = 2.4, *p*-$C_{Ph'}$), 132.7 (d, $^2J_{CP}$ = 10.3, *o*-C_{Ph}), 132.2 (d, $^2J_{CP}$ = 11.3, *o*-$C_{Ph'}$), 131.1 (d, $^5J_{CP}$ = 0.8, *i*-C_{Tol-Me}), 130.0 (s, β-CH_{Tol}), 129.9 (d, $^3J_{CP}$ = 12.3, *m*-C_{Ph}), 129.0 (d, $^3J_{CP}$ = 11.7, *m*-$C_{Ph'}$), 128.6 (d, $^1J_{CP}$ = 105.2, *i*-C_{Ph}), 126.8 (d, $^1J_{CP}$ = 80.6, *i*-$C_{Ph'}$), 123.4 (d, $^3J_{CP}$ = 8.6, α-CH_{Tol}), 121.2 (s, *i*-C_{Cym}), 119.5 (s, *i*-C_{Cym}), 97.8 (s, CH_{Cym}), 95.2 (s, CH_{Cym}), 32.1 (s, *CH*Me_2), 22.7 (s, CH*Me*$_2$), 20.6 (s, Me_{Tol}), 19.5 (s, Me_{Cym}). IR (CH_2Cl_2, ν, cm^{-1}): 2012 (RuCO). UV-vis (CH_2Cl_2; λ_{max}, nm; ε, $M^{-1}\,cm^{-1}$): 480 (140).

EXSY ^{1}H NMR. 2D ^{1}H-^{1}H EXSY spectra were collected on a Bruker Avance 600 spectrometer at 25°C using the standard Bruker library *noesygpph* pulse program. At least three experiments with different values of the mixing time t_m were performed to find an optimum mixing time, resulting in sufficiently large exchange cross-peaks without significant relaxation contribution. The rate constants $k = k_{AB} + k_{BA}$ for the A ↔ B exchange reactions were calculated using simple two-site model[19] using Equations (1), (2), where k_{AB} and k_{BA} are the rate constants of the direct and inverse reactions, I_{AB}, I_{BA} and I_{AA}, I_{BB} are the cross-peak and the diagonal peak integral intensities, respectively. In case of exchange between equally populated states ($k_{AB} = k_{BA}$), the exchange rate constant is $k_{ex} = k/2$.

$$\boldsymbol{k} = \frac{1}{t_m}\ln\left(\frac{r+1}{r-1}\right) \qquad (1)$$

$$\boldsymbol{r} = \frac{I_{AA}+I_{BB}}{I_{AB}+I_{BA}} \qquad (2)$$

The activation free energy $\Delta G^{\neq}$ was calculated from the Eyring equation (3) and the activation enthalpy $\Delta H^{\neq}$ and entropy $\Delta S^{\neq}$ were derived by linear fitting of $R\ln(k_{ex}/T)$ plotted *vs*. $1/T$ according to the equation (4).

$$\Delta \boldsymbol{G}^{\neq} = -\boldsymbol{RT}\ln\frac{k_{ex}h}{k_bT} \qquad (3)$$

$$\boldsymbol{R}\ln\frac{k_{ex}}{T} = -\frac{\Delta H^{\neq}}{T} + \Delta \boldsymbol{S}^{\neq} + \boldsymbol{R}\ln\frac{k_b}{h} \qquad (4)$$

UV-Vis spectroscopic study. The UV-vis monitored titrations were performed in a 10 mm quartz cell, while the spectra at low temperatures were recorded in a 2.2 mm quartz cell. In most experiments the initial concentrations of ruthenium complex (c^0_{Ru}) were 2.5×10^{-3} M, while in other cases c^0_{Ru} was in the range $5–8\times10^{-4}$ M. Neat MeCN and pyridine were used for the titrations. To calculate the dissociation constants K_d for **1b,c** (Eq. 5) and the constant K_c for the ligand coordination to **2a** (Eq. 6), the equilibrium concentrations of the 16ē ($\boldsymbol{c}_{16ē}$) and 18ē ($\boldsymbol{c}_{18ē}$) complexes were obtained from the UV-vis spectra according to the Beer-Lambert law. The absorption of the equilibrium mixture $D(\lambda_i)$ was measured at a wavelength λ_i (Eq. 7), at which the absorption coefficient $\boldsymbol{\varepsilon}_{18ē}$ for 18ē complexes (**1** or **2a(L)**) is close to zero, while the $\boldsymbol{\varepsilon}_{16ē}$ for 16ē species (**2a-c**) is still high enough. Particularly, at the chosen λ_i = 600 nm, $\boldsymbol{\varepsilon}_{16ē}$ is in the range 550 – 650 $M^{-1}\,cm^{-1}$, whereas $\boldsymbol{\varepsilon}_{18ē}$ is < 30 $M^{-1}\,cm^{-1}$. Therefore, the equilibrium concentration $\boldsymbol{c}_{16ē}$ can be approximated as in Equation (8).

$$\boldsymbol{K_d} = \frac{c_{Ru+}c_{Cl-}}{c_{RuCl}} \qquad (5)$$

$$\boldsymbol{K_c} = \frac{c_{RuL+}}{c_{Ru+}c_L} \qquad (6)$$

$$\boldsymbol{D}(\lambda_i) = \boldsymbol{\varepsilon}_{16ē}(\lambda_i)\boldsymbol{c}_{16ē}\boldsymbol{l} + \boldsymbol{\varepsilon}_{18ē}(\lambda_i)\boldsymbol{c}_{18ē}\boldsymbol{l} \qquad (7)$$

$$\boldsymbol{c}_{16ē} \sim \frac{D(\lambda_{600})}{\varepsilon_{16ē}(\lambda_{600})l} \qquad (8)$$

In the titration of **2a** with L, the initial concentrations $c^0_{16ē}$ of **2a** for every *i*-titration point was corrected for the dilution factor ($\boldsymbol{c}^{\boldsymbol{0}}_{16ē}(\boldsymbol{i})$) according to Equation (9).

$$\boldsymbol{c}^{\boldsymbol{0}}_{16ē}(\boldsymbol{i}) = \boldsymbol{c}^{\boldsymbol{0}}_{16ē}\frac{V^0_{16ē}}{V^0_{16ē}+V_L} \qquad (9)$$

where $\boldsymbol{V}^{\boldsymbol{0}}_{16ē}$ and $\boldsymbol{V}_{\boldsymbol{L}}$ are the initial volume of **2a** solution and the added volume of L, correspondingly.

Computational details. The geometry optimizations were carried out with the PBE functional and def2-TZVP[34] basis set for all atoms without any symmetry restrictions in the gas phase using the Gaussian09 package.[35] The obtained stationary points were confirmed to have no imaginary frequencies. The orbital energies were computed with the SMD[36] solvent model using the gas phase optimized geometry.

X-ray crystal structure determination. Single crystals **1d**, **2d**, **3a**, **3c**, **3d** were obtained by slow diffusion of Et_2O into CH_2Cl_2 solutions; in the case of **3d** the solution was saturated with CO. The data collection for samples **1d** and **2d** were performed on a Bruker APEX DUO diffractometer, and those for **3a**, **3c** and **3d** on a Bruker SMART APEX II diffractometer, both equipped with an Apex II CCD detector and operating with MoKα radiation (λ = 0.71073 Å). Frames were integrated using the Bruker SAINT software package[37] by a narrow-frame algorithm. A semiempirical absorption correction was applied with the SADABS[38] program using the intensity data of equivalent reflections. The structures were solved with direct methods and refined by the full-matrix least-squares technique against F^2_{hkl} in anisotropic approximation with the SHELX[39] software package. The positions of the hydrogen atoms were calculated, and all hydrogen atoms were refined using the riding model with 1.5Ueq(Cm) and 1.2Ueq(Ci), where Ueq(Cm) and 1.2Ueq(Ci) are respectively the equivalent thermal parameters of methyl and all other carbon atoms to which corresponding H atoms are bonded. The structure of **1d** contains an interstitial CH_2Cl_2 molecule, which is disordered about an inversion center. In the structure of **3d** two crystallographically independent cations and anions are related by an approximate non-crystallographic inversion center. Detailed crystallographic information is given in Table 4. Crystallographic data have been deposited to the Cambridge Crystallographic Data Centre, CCDC numbers 1536180-1536184. Copies of the data can be obtained free of charge via http://www.ccdc.cam.ac.uk/data_request/cif, or by e-mailing data_request@ccdc.cam.ac.uk, or by contacting The Cambridge Crystallographic Data Centre, 12 Union Road, Cambridge CB2 1EZ, UK; fax: +44(0)1223-336033.

Table 3. Crystal data and structure refinement parameters for **1d**, **2d**, **3a**, **3c**, **3d**.

	1d	**2d**	**3a**	**3c**	**3d**
Formula	$C_{36.50}H_{39}Cl_2N_2PRu$	$C_{36}H_{38}F_6N_2P_2Ru$	$C_{39}H_{42}F_6N_2OP_2Ru$	$C_{28}H_{34}F_6N_2O_2P_2Ru$	$C_{37}H_{38}F_6N_2OP_2Ru$
Formula weight	708.63	775.69	831.75	707.58	803.70
T, K	120	120	100	120	120
Crystal system	monoclinic	monoclinic	monoclinic	monoclinic	monoclinic
Space group	$P2_1/c$	$P2_1/c$	$P2_1/n$	$P2_1/n$	Pn
Z / Z'	4 / 1	4 / 1	4 / 1	4 / 1	4 / 2
a, Å	9.4575(3)	9.4269(5)	9.6577(7)	14.1458(9)	10.2091(7)
b, Å	23.0562(8)	19.0924(11)	20.7348(15)	12.0157(8)	10.0913(8)
c, Å	14.5931(5)	19.2392(11)	18.7465(14)	18.3241(12)	34.401(3)
β, °	98.659(2)	92.5880(10)	94.0820(16)	99.2530(10)	96.029(2)
V, Å^3	3145.81(18)	3459.2(3)	3744.5(5)	3074.1(3)	3524.5(4)
d_{calc}, g cm^{-3}	1.496	1.489	1.475	1.529	1.515
μ, cm^{-1}	7.49	6.07	5.68	6.79	6.00
$2\theta_{max}$, °	60	54	60	60	58
Reflns. collected / independent	64054 / 9170	47949 / 7492	38229 / 10895	38560 / 8962	27738 / 14871
Observed reflections [I>2σ(I)]	6614	6101	7163	7722	11444
R_1	0.0461	0.0455	0.0475	0.0438	0.0514
wR_2	0.1077	0.0918	0.1039	0.1182	0.0829
GOF	1.052	1.085	1.015	1.079	1.014
Residual density, e Å^{-3} (d_{max}/d_{min})	0.515/-0.916	0.880/-0.646	0.845/-0.563	1.593/-0.750	0.724/-0.695

Acknowledgements

The authors thank the Russian Science Foundation (grant no. 14-13-00801) for financial support. I.S. thanks the French Ministry of Foreign Affairs for a Ph.D. scholarship through the French Embassy in Moscow.

Keywords: ruthenium iminophosphonamides • electron-deficient complexes • carbonyl complexes • CO insertion • 2D EXSY NMR

[1] T. Naota, H. Takaya, S.-I. Murahashi, *Chem. Rev.* **1998**, *98*, 2599-2660.
[2] R. Poli, *Chem. Rev.* **1996**, *96*, 2135-2204.
[3] T.J. Johnson, K. Folting, W.E. Streib, J.D. Martin, J.C. Huffman, S.A. Jackson, O. Eisenstein, K.G. Caulton, *Inorg. Chem.* **1995**, *34*, 488-499.
[4] A.D. Phillips, G. Laurenczy, R. Scopelliti, P.J. Dyson, *Organometallics* **2007**, *26*, 1120-1122.
[5] A.D. Phillips, O. Zava, R. Scopelitti, A.A. Nazarov, P.J. Dyson, *Organometallics* **2010**, *29*, 417-427.
[6] A.D. Phillips, K. Thommes, R. Scopelliti, C. Gandolfi, M. Albrecht, K. Severin, D.F. Schreiber, P.J. Dyson, *Organometallics* **2011**, *30*, 6119-6132.
[7] P. Dejan, G. Thomas, B. Thomas, G.H. Cristian, R. Sören, G.J. Peter, T. Matthias, *Eur. J. Inorg. Chem.* **2007**, 3472-3475.
[8] T. Glöge, D. Petrovic, C. Hrib, P.G. Jones, M. Tamm, *Eur. J. Inorg. Chem.* **2009**, 4538-4546.
[9] Y. Yamaguchi, H. Nagashima, *Organometallics* **2000**, *19*, 725-727.
[10] T. Hayashida, Y. Yamaguchi, K. Kirchner, H. Nagashima, *Chem. Lett.* **2001**, 954-955.
[11] H. Kondo, Y. Yamaguchi, H. Nagashima, *J. Am. Chem. Soc.* **2001**, *123*, 500-501.
[12] H. Nagashima, H. Kondo, T. Hayashida, Y. Yamaguchi, M. Gondo, S. Masuda, K. Miyazaki, K. Matsubara, K. Kirchner, *Coord. Chem. Rev.* **2003**, *245*, 177-190.
[13] J.I. Terasawa, H. Kondo, T. Matsumoto, K. Kirchner, Y. Motoyama, H. Nagashima, *Organometallics* **2005**, *24*, 2713-2721.
[14] T.A. Peganova, A.V. Valyaeva, A.M. Kalsin, P.V. Petrovskii, A.O. Borissova, K.A. Lyssenko, N.A. Ustynyuk, *Organometallics* **2009**, *28*, 3021-3028.
[15] T.A. Peganova, I.S. Sinopalnikova, A.S. Peregudov, I.V. Fedyanin, A. Demonceau, N.A. Ustynyuk, A.M. Kalsin, *Dalton Trans.* **2016**, *45*, 17030-17041.
[16] P.J. Bailey, K.J. Grant, S. Parsons, *Organometallics* **1998**, *17*, 551-555.
[17] S. Tsukada, T. Sagawa, T. Gunji, *Chem. Asian J.* **2015**, *10*, 1881-1883.
[18] N.V. Belkova, L.M. Epstein, E.S. Shubina, *Eur. J. Inorg. Chem.* **2010**, 3555-3565.
[19] A.D. Bain, *Prog. Nucl. Magn. Reson. Spectrosc.* **2003**, *43*, 63-103.
[20] C.L. Perrin, T.J. Dwyer, *Chem. Rev.* **1990**, *90*, 935-967.
[21] Although the Van't Hoff plot for **1d** allowed us to find the entropy term ΔS = -18.7±0.4 cal/(mol•K), it requires correction for chloride concentration. In

fact it consists of $\Delta S_{ex}^{\neq}$ and the constant $R\ln[Cl^-]$ as the rate of associtive process depends on the concentration of the Cl^-. Since the stationary $[Cl^-]$ is unknown the true $\Delta S_{ex}^{\neq}$ cannot be calculated. Nevertheless, the calculated activation enthalpy $\Delta H_{ex}^{\neq}$ does not require any correction due to the change of the mechanism.

[22] K. Mashima, H. Kaneyoshi, S.-I. Kaneko, A. Mikami, K. Tani, A. Nakamura, *Organometallics* **1997**, *16*, 1016-1025.

[23] R.S. Rowland, R. Taylor, *J. Phys. Chem.* **1996**, *100*, 7384-7391.

[24] C. Gemel, J.C. Huffman, K.G. Caulton, K. Mauthner, K. Kirchner, *J. Organomet. Chem.* **2000**, *593–594*, 342-353.

[25] A. Zamorano, N. Rendón, J.E.V. Valpuesta, E. Álvarez, E. Carmona, *Inorg. Chem.* **2015**, *54*, 6573-6581.

[26] C.J. Adams, R.A. Baber, N.G. Connelly, P. Harding, O.D. Hayward, M. Kandiah, A.G. Orpen, *Dalton Trans.* **2007**, 1325-1333.

[27] C. Jones, C. Schulten, R.P. Rose, A. Stasch, S. Aldridge, W.D. Woodul, K.S. Murray, B. Moubaraki, M. Brynda, G. La Macchia, L. Gagliardi, *Angew. Chem. Int. Ed.* **2009**, *48*, 7406-7410.

[28] T.J.J. Sciarone, C.A. Nijhuis, A. Meetsma, B. Hessen, *Organometallics* **2008**, *27*, 2058-2065.

[29] H. Brunner, J. Wachter, *J. Chem. Res. (S)* **1978**, 136-137.

[30] E. Jellema, T.J.J. Sciarone, N.M. Navarrete, M.J. Hettinga, A. Meetsma, B. Hessen, *Eur. J. Inorg. Chem.*, **2011**, 91-100.

[31] Ö. Öztopcu, B. Stöger, K. Mereiter, K. Kirchner, *J. Organomet. Chem.* **2013,** *735*, 80-87.

[32] T. Hayashida, H. Nagashima, *Organometallics* **2001**, *20*, 4996-4998.

[33] S.B. Jensen, S.J. Rodger, M.D. Spicer, *J. Organomet. Chem.* **1998**, *556*, 151-158.

[34] F. Weigend, R. Ahlrichs, *Phys. Chem. Chem. Phys.* **2005**, *7*, 3297-3305.

[35] M.J. Frisch, G.W. Trucks, H.B. Schlegel, G.E. Scuseria, M.A. Rob, J.R. Cheeseman, J.A.M. Jr, T. Vreven, K.N. Kudin, J.C. Burant, J.M. Millam, S.S. Iyengar, J. Tomasi, V. Barone, B. Mennucci, M. Cossi, G. Scalmani, N. Rega, G.A. Petersson, H. Nakatsuji, M. Hada, M. Ehara, K. Toyota, R. Fukuda, J. Hasegawa, M. Ishida, T. Nakajima, Y. Honda, O. Kitao, H. Nakai, M. Klene, X. Li, J.E. Knox, H.P. Hratchian, J.B. Cross, V. Bakken, C. Adamo, J. Jaramillo, R. Gomperts, R.E.Stratmann, O. Yazyev, A.J. Austin, R. Cammi, C. Pomelli, J.W. Ochterski, P.Y. Ayala, K. Morokuma, G.A. Voth, P. Salvador, J.J. Dannenberg, V.G. Zakrzewski, S. Dapprich, A.D. Daniels, M.C. Strain, O. Farkas, D.K. Malick, A.D. Rabuck, K. Raghavachari, J.B. Foresman, J.V. Ortiz, Q. Cui, A.G. Baboul, S. Clifford, J. Cioslowski, B.B. Stefanov, G. Liu, A. Liashenko, P. Piskorz, I. Komaromi, R.L. Martin, D.J. Fox, T. Keith, M.A. Al-Laham, C.Y. Peng, A. Nanayakkara, M. Challacombe, P.M.W. Gill, B. Johnson, W. Chen, M.W. Wong, C. Gonzalez, J.A. Pople. *Gaussian 09, Revision D.01. Gaussian, Inc., Wallingford, CT, 2009*, 2009.

[36] A.V. Marenich, C.J. Cramer, D.G. Truhlar, *J. Phys. Chem. B* **2009**, *113*, 6378-6396.

[37] *SAINT v8.34A., Bruker AXS, Madison, Wisconsin, USA*, 2013.

[38] G.M. Sheldrick. *SADABS,* v. 2.03, Bruker/Siemens Area Detector Absorption Correction Program, Bruker AXS, Madison, Wisconsin, 2003.

[39] G.M. Sheldrick, *Acta Crystallogr. C* **2015**, *C71*, 3-8.

Entry for the Table of Contents

FULL PAPER

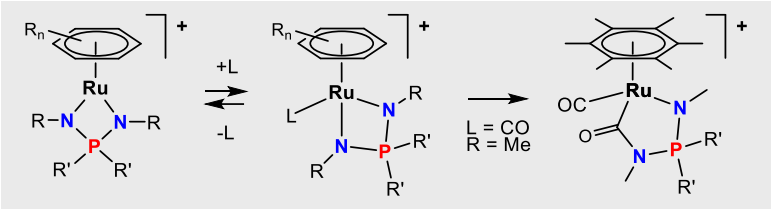

The lone pair of the highly basic iminophosphonamide N-atoms in arene ruthenium complexes can both stabilize 16ē species and attack an external ligand in 18ē species.

*Iana S. Sinopalnikova, Tat'yana A. Peganova, Valentin V. Novikov, Ivan V. Fedyanin, Oleg A. Filippov, Natalia V. Belkova, Elena S. Shubina, Rinaldo Poli, Alexander M. Kalsin**

Page No. – Page No.

Coordinatively labile 18-electron arene ruthenium iminophosphonamide complexes

Keywords: Arene ruthenium complexes, iminophosphonamides, electron-deficient compounds, N ligands, organometallic chemistry